Tension-stiffening concept of reinforced concrete surface structures

Autor(en): **Mang, H.A. / Floegl, H.**

Objekttyp: **Article**

Zeitschrift: **IABSE reports of the working commissions = Rapports des commissions de travail AIPC = IVBH Berichte der Arbeitskommissionen**

Band (Jahr): **34 (1981)**

PDF erstellt am: **05.08.2024**

Persistenter Link: https://doi.org/10.5169/seals-26901

Tension-Stiffening Concept for Reinforced Concrete Surface Structures

Tension-stiffening concept pour des constructions en surfaces porteuses en béton armé

Tension-Stiffening Konzept für Flächentragwerke aus Stahlbeton

H.A. MANG
Associate Professor

H. FLOEGL
Research Associate

Institut für Baustatik und Festigkeitslehre der TU-Wien
Wien, Österreich

SUMMARY

Disregard of the capacity of the concrete between neighboring cracks to carry tensile forces normal to the cracks - the so-called "tension-stiffening effect" - may result in underestimating member stiffnesses considerably. In this paper, a novel tension stiffening concept for reinforced concrete surface structures is presented. It is based on bond slip between the reinforcement and the surrounding concrete. Good agreement of results from geometrically and physically nonlinear finite-element-analyses with experimental results is demonstrated.

RÉSUMÉ

En négligeant la capacité du béton de transmettre des forces de traction perpendiculairement à la direction des fissures - qu'on appelle le "Tension-Stiffening Effect" - on sous-estime la rigidité des membres portants. Dans la publication qui suit on présente une nouvelle méthode de tenir compte du "Tension-Stiffening" pour des constructions en surfaces porteuses (dalles, coques, etc.) en béton armé. La méthode est basé sur les déformations relatives entre les barres d'acier et le béton. Les résultats des calculs non-linéaires (géometriquement et physiquement), faits avec l'aide de la méthode des éléments finis correspondent bien avec les résultats d'essais, connus d'autres publications.

ZUSAMMENFASSUNG

Die Nichtberücksichtigung der Kapazität des Betonzwischen benachbarten Rissen, Zugkräfte normal zu den Rissen aufzunehmen - des sogenannten "Tension-Stiffening Effekts" - kann zu einer beträchtlichen Unterschätzung der Steifigkeit von Traggliedern führen. In der vorliegenden Arbeit wird ein neuartiges Tension-Stiffening Konzept für Flächentragwerke aus Stahlbeton präsentiert. Es beruht auf Gleitverbund zwischen der Bewehrung und dem umgebenden Beton. Die Ergebnisse zufolge geometrisch und physikalisch nichtlinearer Berechnungen mittels der Methode der Finiten Elemente stimmen gut mit experimentellen Vergleichsresultaten aus der Literatur überein.

1. INTRODUCTION

The capacity of the concrete between neighboring cracks to carry tensile stresses, transferred from the reinforcement to the surrounding cracks is termed "tension-stiffening effect". The vehicle for this stress transfer is bond slip between the reinforcement and the surrounding concrete. If tension stiffening is disregarded, ultimate load analysis of reinforced concrete (RC) surface structures may result in average steel stresses between neighboring cracks which are too large. The ultimate load may be underestimated considerably.

In the course of the last years, a number of analytical models for consideration of tension stiffening have been proposed. With regard to thin slabs, more recently Gilbert and Warner [1] have reviewed some of these models which can be characterized as "strain-softening approaches". Fig.1, taken from [1], shows typical modified stress-strain diagrams for two different models for consideration of tension stiffening.

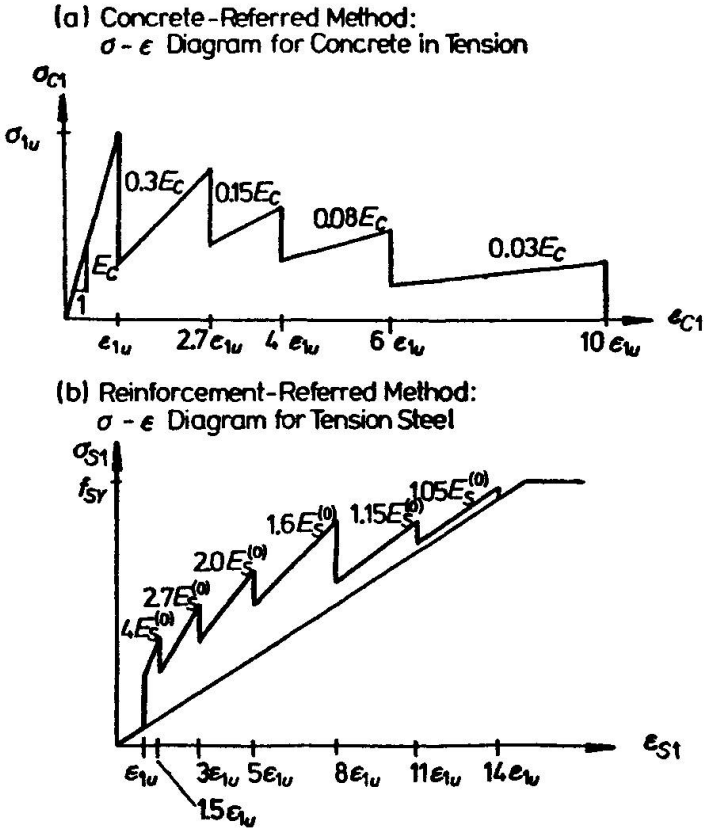

Fig.1 Modified Stress-Strain Diagrams for Consideration of Tension Stiffening (Ref.1)

Fig.1(a) illustrates the relationship between the average concrete tensile strain normal to neighboring parallel cracks, ε_{C1}, and the corresponding stress, σ_{C1}, for the so-called "concrete-referred method" [2], as proposed by Scanlon [3]. The quantities ε_{1u} and σ_{1u} denote the strain and the stress at initial cracking; E_C is the elastic modulus of concrete in uniaxial tension. Gilbert and Warner [1] have discussed modifications of this method.

Fig.1(b) shows a modified stress-strain diagram for steel in tension after cracking of concrete as used within the framework of the so-called "reinforcement-referred method" [2]. This method was proposed by Gilbert and Warner [1]. In Fig.1(b), ε_{S1}, $E_S^{(0)}$, σ_{S1} and f_{SY} denote the average steel strain between neighboring cracks, the elastic modulus of steel, the average steel stress and the yield stress of the reinforcement.

Both methods do not consider the influence of the angle between the crack and the intersecting reinforcement bar. Moreover, the influence of crack propagation through the thickness of slabs and shells on the tension-stiffening effect is not dealt with adequately, since it is not controlled by the coordinate normal to the middle surface of the shell.

The writers' purpose is to report on the essential features of a novel analytical concept within the framework of the Finite Element Method (FEM) for consideration of tension stiffening in thin RC surface structures, based on bond slip between the reinforcement and the surrounding concrete [2], [4]. It is characterized by approximate consideration of the influence of (a) the angle between the crack and the intersecting reinforcement bar, (b) crack propagation through the thickness of the shell, and (c) secondary cracks between neighboring primary cracks on the tension stiffening effect. Nonlinearity of concrete, strain-hardening plasticity of steel, geometric nonlinearity and the dependence of hydrostatic pressure on the state of deformation is taken into account.

The developed concept is applied to predict the short-term behavior of an RC panel and an RC shell, for both of which experi-

mental results are available in the literature.

2. THEORETICAL CONCEPT

2.1 Equilibrium Equations

Fig.2 shows the middle surface S of an undeformed RC shell with the boundary Γ. It also illustrates the deformed shell (middle surface S', boundary Γ'). The shell is subdivided into m C^o-conforming, curved, triangular finite elements each of which consists of n thin layers such that, approximately, a plane state of stress may be assumed in each layer. The thickness of layer ℓ is given

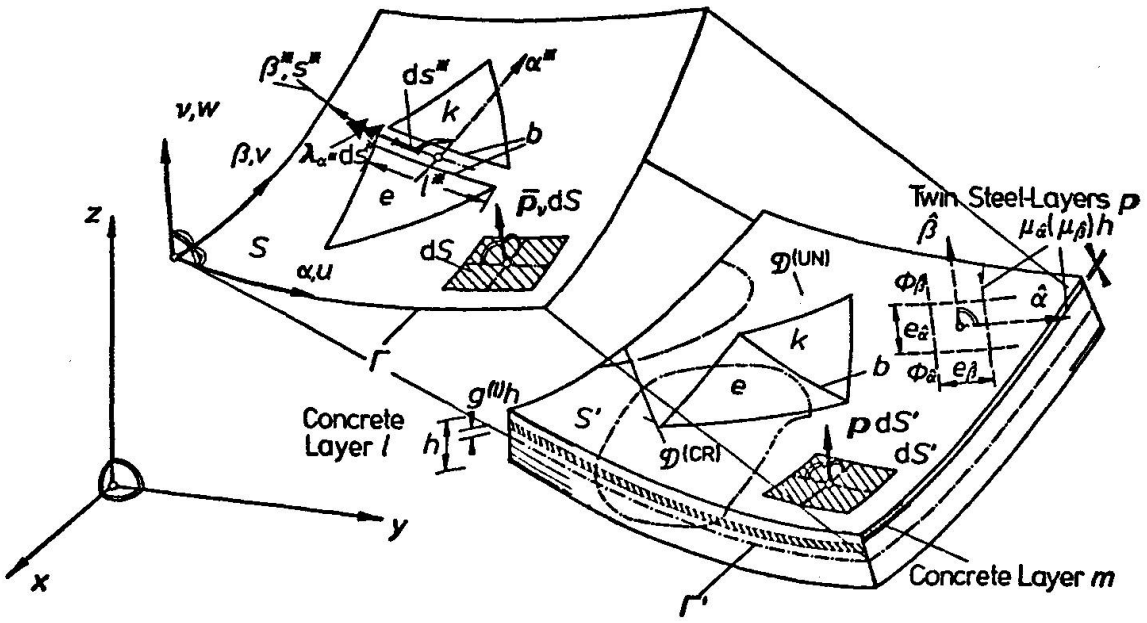

Fig.2 Middle Surface of Undeformed RC Shell; Layered Finite Element Model of Deformed, Partially Cracked Shell

as $g^{(\ell)}h$, where h is the thickness of the shell and $g^{(\ell)}$ is the weight coefficient for Gauss integration. Fig.2 contains global Cartesian coordinates, x,y,z, global surface coordinates, α,β,ν, local surface coordinates, α^*,β^*, referred to the common boundary

b of two neighboring elements, e and k, and local surface coordinates, $\hat{\alpha}$, $\hat{\beta}$, parallel to an orthogonal net of reinforcement bars with diameters $\hat{\phi}_\alpha$, $\hat{\phi}_\beta$. The bars are "smeared" to "twin steel-layers" with thicknesses $\mu_{\hat{\alpha}}(\mu_{\hat{\beta}})h$, where $\mu_{\hat{\alpha}}(\mu_{\hat{\beta}})$ are the degrees of reinforcement. In addition to dead load, the shell is assumed to be loaded by hydrostatic pressure (undeformed configuration: $\bar{p}_\nu dS$, deformed configuration: $p\,dS'$); $\lambda_{\alpha^*} ds^*$ is an unknown distributed bending moment, required for enforcing C^1-continuity at b; u, v, w are components of the displacement vector parallel to α, β, ν. The symbols $\mathcal{D}^{(UN)}$ and $\mathcal{D}^{(CR)}$ denote the entirety of uncracked and cracked subregions of the shell. To talk of such subregions is only meaningful if a "smeared-crack concept" is applied as is done in the given case.

The equations of equilibrium are given as [4]

$$\sum_{e=1}^{m}\Big[\sum_{\ell=1}^{n} g^{(\ell)}\Big(\int_{S_C^{(e,\ell;UN)}} \sigma_{i''}\,\delta\varepsilon_{i''}\,h\,dS + \int_{S_C^{(e,\ell;CR)}} \sigma^{(a)}_{i'j'}\,\delta\varepsilon^{(a)}_{i'j'}\,h\,dS\Big) +$$

$$+\sum_{p=1}^{r}\Big(\int_{S_{S\hat{\imath}}^{(e,p;UN)}} \sigma_{\hat{\imath}}\,\delta\varepsilon_{\hat{\imath}}\,\mu_{\hat{\imath}}\,h\,dS + \int_{S_{S\hat{\imath}}^{(e,p;CR)}} \sigma^{(a)}_{\hat{\imath}}\,\delta\varepsilon^{(a)}_{\hat{\imath}}\,\mu_{\hat{\imath}}\,h\,dS - \int_{\sum \ell_{\hat{\imath}}^{(e,p;CR)}} t^{(a)}_{B\hat{\imath}}\,\delta u^{(a)}_{R\hat{\imath}}\,ds_{\hat{\imath}}\Big) -$$

$$-\int_{V^{(e)}} \bar{p}_g\,\delta u_g\,dV - \int_{S_p^{(e)}} p_g\,\delta u_g\,dS\Big] - \sum_{b=1}^{q}\int_{\ell^*(b)}\left(\lambda_{1^*}\,\delta\vartheta_{1^*} + \vartheta_{1^*}\,\delta\lambda_{1^*}\right)ds^* = 0,$$

$$g = 1, 2, 3;\quad i,j = 1,2;\quad 1\equiv\alpha,\ 2\equiv\beta,\ 3\equiv\nu. \qquad (1)$$

The first integral in (1) represents the virtual work of the internal forces acting in the part of concrete layer ℓ of element e which belongs to $\mathcal{D}^{(UN)}$. The respective part of the middle surface of layer ℓ is denoted as $S_C^{(e,\ell;UN)}$; $\varepsilon_{i''}$ and $\sigma_{i''}$ are the strains and stresses in the principal directions, α'', β''. The transfer from displacements to strains is accomplished by means of a theory of small strains but moderately large rotations, developed by Koiter [5]. Biaxial stress-strain relations, proposed by Liu, Nilson and Slate [6] on the basis of experiments of Kupfer [7] are used.

The second integral in (1) extends over $S_C^{(e,\ell;CR)}$, which is part of $\mathcal{D}^{(CR)}$; $\varepsilon^{(a)}_{i'j'}$ and $\sigma^{(a)}_{i'j'}$ are average strains and stresses

normal and parallel to cracks. Within tributary domains of Gauss points for numerical integration, the cracks are assumed to be parallel and equidistant. Only two crack bands are taken into account. For reasons of simplicity, the second crack band is assumed to be normal to the first one. The directions of the normals to the two crack bands are denoted as α' , β' .

The third and the fourth integral in (1) refer to the reinforcement steel in "twin steel-layers" p ; $S_{S\hat{\imath}}^{(e,p;UN)}$ ($S_{S\hat{\imath}}^{(e,p;CR)}$) denotes the part(s) of the middle surface(s) p which are located in $\mathcal{D}^{(UN)}$ ($\mathcal{D}^{(CR)}$); $\varepsilon_{\hat{\imath}}^{(a)}$ and $\sigma_{\hat{\imath}}^{(a)}$ are average strains and stresses in the directions of the reinforcement bars, $\hat{\alpha}$, $\hat{\beta}$.

The integrand of the fifth integral in (1) represents the virtual work done by average bond forces $t_{B\hat{\imath}}^{(a)}$, given as

$$t_{B\hat{\imath}}^{(a)} = \tau_{B\hat{\imath}}^{(a)} \phi_{\hat{\imath}} \pi , \qquad \hat{\imath} = \hat{1},\hat{2} \text{ (no summation)}; \hat{1} \equiv \hat{\alpha}, \hat{2} \equiv \hat{\beta}, \quad (2)$$

where $\tau_{B\hat{\imath}}^{(a)}$ are average bond stresses, on virtual average bond slips, $\delta u_{R\hat{\imath}}^{(a)}$. In the context of concrete-frame analysis, Åldstedt and Bergan [16] have considered an analogous virtual-work term.

Assuming full bond in $\mathcal{D}^{(UN)}$, the aforementioned integral stretches only over those parts of the reinforcement bars which are located in $S_{S\hat{\imath}}^{(e,p;CR)}$. The domain of integration is written symbolically as $\sum \ell_{\hat{\imath}}^{(e,p;CR)}$, where $\ell_{\hat{\imath}}^{(e,p;CR)} \equiv \ell_{\hat{\imath}}$ are lengths of reinforcement bars between neighboring cracks in $S_{S\hat{\imath}}^{(e,p;CR)}$ [4].

Fig.3 contains a comparison of "actual" stress distributions between neighboring parallel cracks with idealized stress distributions employed for the analysis; $\tau_{B\hat{\imath}}^{(a)}$ represents the average value of $\tau_{B\hat{\imath}}$. Note that $\sigma_{C\hat{\imath}\hat{\imath}}^{(a)}$ and $\sigma_{S\hat{\imath}}^{(a)}$ are not average values of $\sigma_{C\hat{\imath}\hat{\imath}}$ and $\sigma_{S\hat{\imath}}$.

On the basis of Fig.3, the average bond slip between neighboring cracks, $u_{R\hat{\imath}}^{(a)}$, is obtained as

$$u_{R\hat{\imath}}^{(a)} = \Delta_{S\hat{\imath}}^{(a)} - \Delta_{C\hat{\imath}}^{(a)} = \left(\varepsilon_{S\hat{\imath}}^{(a)} - \varepsilon_{C\hat{\imath}\hat{\imath}}^{(a)}\right) \frac{\ell_{\hat{\imath}}}{4} \quad (3)$$

where

$$\Delta_{S\hat{\imath}}^{(a)} = \frac{1}{2}\left[u_{S\hat{\imath}}(s_{\hat{\imath}} = \ell_{\hat{\imath}}/2) - u_{S\hat{\imath}}(s_{\hat{\imath}} = 0)\right] \quad (4.1)$$

and

$$\Delta_{C\hat{i}}^{(\sigma)} = \frac{1}{2}\left[u_{C\hat{i}}(s_{\hat{i}} = \ell_{\hat{i}}/2) - u_{C\hat{i}}(s_{\hat{i}} = 0)\right] \tag{4.2}$$

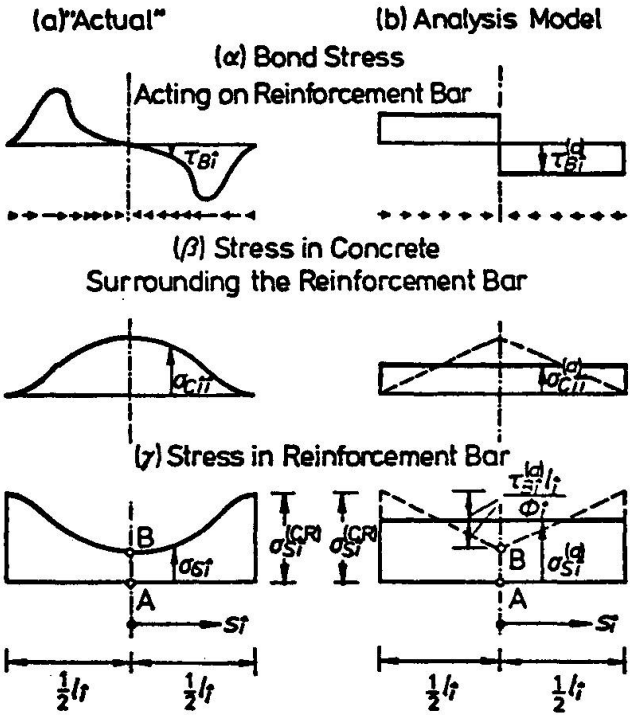

Fig.3 "Actual" and Idealized Stress Distributions

In case of cracks which are non-orthogonal to the reinforcement bars, $\ell_{\hat{i}}$ may exceed the boundaries of the tributary domain of the considered integration point. In case of such cracks, kinking of the reinforcement will occur at cracks, resulting in a reduction of bond slip. This suggests replacing (3) by

$$u_{R\hat{i}}^{(\sigma)} = \Delta_{S\hat{i}}^{(\sigma)} - \Delta_{C\hat{i}}^{(\sigma)} \tag{5}$$

where $|\Delta_{S\hat{i}}^{(\sigma)}| \leq |\Delta_{S\hat{i}}^{(\sigma)}|$ and $|\Delta_{C\hat{i}}^{(\sigma)}| \leq |\Delta_{C\hat{i}}^{(\sigma)}|$ and where $\Delta_{S\hat{i}}^{(\sigma)}$ is estimated as follows:

$$\Delta_{S\hat{i}}^{(\sigma)} = \begin{Bmatrix} n_{1'\hat{i}}^2 \\ 1 \end{Bmatrix} \left[\sum_{\ell=1}^{n} g^{(\ell)} \left(1 + \frac{12\,\nu_{S\hat{i}}}{h^2} \nu_C^{(\ell)} \right) \frac{\ell_{\hat{i}}}{\ell_{\hat{i}}^{(\ell)}} \right] \varepsilon_{S\hat{i}}^{(\sigma)} \frac{\ell_{\hat{i}}}{4} . \tag{6}$$

For parallel cracks in one direction (see Fig.4),

$$\ell_{\hat{i}} = \frac{b_{1'}}{|n_{1'\hat{i}}|} , \qquad \ell_{\hat{i}}^{(\ell)} = \frac{b_{1'}^{(\ell)}}{|n_{1'\hat{i}}^{(\ell)}|} , \tag{7.1}$$

and for parallel cracks in two directions (see Fig.4),

$$\ell_{\hat{\imath}} = \frac{b_{1'} b_{2'}}{b_{1'} |n_{2'\hat{\imath}}| + b_{2'} |n_{1'\hat{\imath}}|}, \qquad \ell_{\hat{\imath}}^{(\ell)} = \frac{b_{1'}^{(\ell)} b_{2'}^{(\ell)}}{b_{1'}^{(\ell)} |n_{2'\hat{\imath}}^{(\ell)}| + b_{2'}^{(\ell)} |n_{1'\hat{\imath}}^{(\ell)}|} \,. \tag{7.2}$$

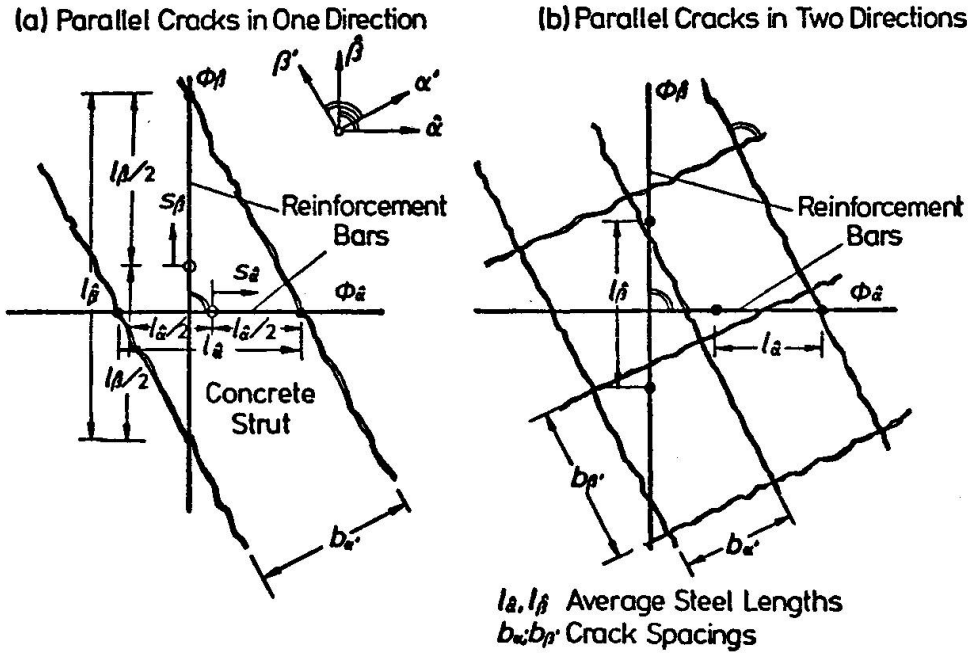

Fig.4 Reinforcement Bars Intersecting Crack Bands in One or Two Directions

Note that for parallel cracks in two directions, $\ell_{\hat{\imath}}$ ($\ell_{\hat{\imath}}^{(\ell)}$) are average quantities. In (7.2), $b_{1'}$ and $b_{2'}$ denote crack spacings in the concrete layer containing the considered steel layer; $n_{1'\hat{\imath}}$ and $n_{2'\hat{\imath}}$ are the direction cosines of angles enclosed by the normals to the cracks and the reinforcement bars in the mentioned concrete layer. The quantities $b_{1'}^{(\ell)}$, $b_{2'}^{(\ell)}$, $n_{1'\hat{\imath}}^{(\ell)}$ and $n_{2'\hat{\imath}}^{(\ell)}$ refer to concrete layer ℓ; $z_{S\hat{\imath}}$ ($z_C^{(\ell)}$) is the distance of the considered steel layer (concrete layer ℓ) from the middle surface of the shell. The upper (lower) quantity in the factor $\begin{Bmatrix} n_{1'\hat{\imath}}^2 \\ 1 \end{Bmatrix}$ in (5) refers to parallel cracks in one (two) direction(s).

The crack spacings $b_{\hat{\imath}'}$, are influenced, to a different degree, by various physical parameters of which the concrete strain normal to the crack, $\varepsilon_{C\hat{\imath}'}$, is believed to be the most important one. For the present investigation, according to [2], [4],

$$b_{i'} = 1{,}5\, b_{i'}^{(1)} \left(\frac{\varepsilon_{Ci'i'}}{\varepsilon_{Ctu}}\right)^{-\left(\frac{\log 2}{\log \varrho}\right)} \tag{8}$$

where

$$\varrho = \frac{\varepsilon_{Ci'i'}^{(r+1;a)}}{\varepsilon_{Ci'i'}^{(r;a)}} = \left(\frac{\bar{\varepsilon}_{SY}}{\varepsilon_{Ctu}}\right)^{\frac{1}{s-1}} \qquad j \tag{9}$$

$\varepsilon_{Ci'i'}^{(r;a)}$, r=1,2,...s, denotes average concrete strains at the formation of cracks of order r. In this terminology, r=1 refers to primary cracks; s is the order of cracks assumed to open at initial yield of the reinforcement steel, $\bar{\varepsilon}_{SY}$ is the strain at incipient yield of the reinforcement steel; ε_{Ctu} stands for the uniaxial ultimate tensile strain. Fig.5 shows a plot of $b_{i'}^{(1)}$ versus $\varepsilon_{Ci'i'}^{(a)} \equiv \varepsilon_{i'i'}^{(a)}$.

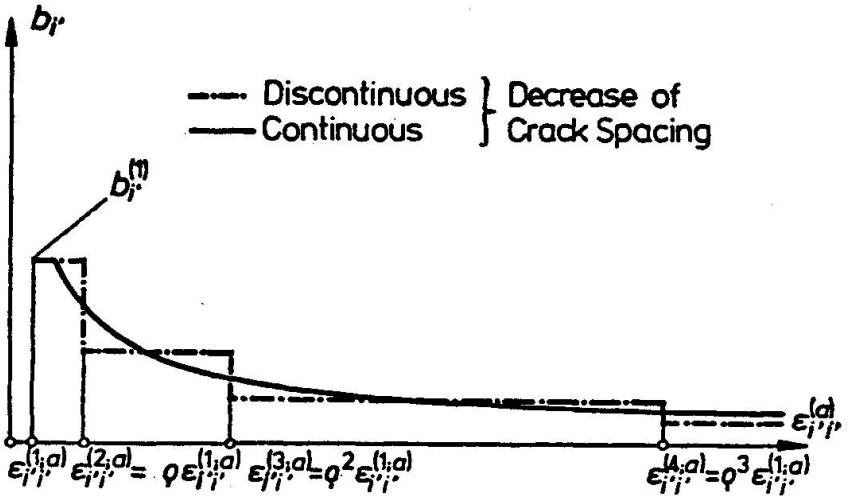

Fig.5 Crack Spacing as a Function of Average Strain Normal to Crack

Substituting (6) into (5), permits writing the integrand of the fifth integral in (1) as follows:

$$t_{B\hat{i}}^{(a)}\,\delta u_{R\hat{i}}^{(a)} = -\Bigg[\frac{|\tau_{B\hat{i}}^{(a)}|}{\sigma_{S\hat{i}}^{(a)}}\frac{\left\{\frac{b_{i'}}{\ell_{\hat{i}}}\right\}}{\phi_{\hat{i}}}\sum_{\ell=1}^{n} g^{(\ell)}\left(1+\frac{12\,\nu_{S\hat{i}}}{h^2}\,\nu_C^{(\ell)}\right)\frac{\left\{\frac{b_{i'}}{\ell_{\hat{i}}}\right\}}{\ell_{\hat{i}}^{(\ell)}}\Bigg]\sigma_{S\hat{i}}^{(a)}\,\delta c_{S\hat{i}}^{(a)}\,\frac{\phi_{\hat{i}}\,\pi}{4} + \\ + |\,t_{B\hat{i}}^{(a)}|\;\delta|\Delta_{C\hat{i}}^{(a)}|\,, \tag{10}$$

$-\ell_{\hat{i}}/2 \le s_{\hat{i}} \le \ell_{\hat{i}}/2$; $\hat{i}=\hat{1},\hat{2}$ (no summation); $\hat{1}\equiv\hat{\alpha}$, $\hat{2}\equiv\hat{\beta}$, $i'\equiv\alpha'$,

where

$$|\tau_{B\hat{i}}^{(a)}| = \left[0{,}07 + 0{,}16\left(\frac{\varepsilon_{S\hat{i}}^{(a)}\left\{\frac{b_{i'}}{\ell_{\hat{i}}}\right\}}{2}\right)^{0.3}\right]|f_{cu}| + 0{,}2\,|\sigma_{C\hat{j}\hat{j}}|, \quad \hat{i}\neq\hat{j}, \tag{11}$$

$\hat{i},\hat{j} = \hat{1},\hat{2}$ (no summation); $\hat{1}\equiv\hat{\alpha}$, $\hat{2}\equiv\hat{\beta}$.

The right side of (11) is an approximation to $|\tau_{B\hat{\imath}}^{(a)}|$. The original expression for $|\tau_{B\hat{\imath}}^{(a)}|$ was derived by Grelat and Potucek [8]. In (10) and (11), upper (lower) quantities refer to parallel cracks in one (two) direction(s). In (11), the dimension of $b_{1'}$ and $\ell_{\hat{\imath}}$, respectively, is [mm]; f_{cu} is the uniaxial compressive strength (prism strength) of concrete.

A few words remain to be said about the last three integrals in (1). The sixth integral represents the virtual work of volume forces $\bar{p}_g$. The integral extends over the volume of finite element e, $V^{(e)}$. The seventh integral expresses the virtual work of hydrostatic pressure $p_g(u_i)$ [9]. It stretches over the loaded part of the surface of element e, $S_p^{(e)}$. The last integral in (1) represents the variation of a load potential with $\lambda_{1*}^{(b)} \equiv \lambda_{1*}$ as the load and with $\vartheta_{1*}^{(b)} \equiv \vartheta_{1*}$ as the corresponding "displacement" in the form of the difference of normal slopes of elements e and k at b. The integral extends over the length of b, $l^{*(b)}$.

2.2. Tension Stiffening Factor

In the following, local groups of equilibrating "external" and internal forces in the concrete surrounding two orthogonal reinforcement bars between neighboring cracks will be identified. For a typical group of such equilibrating forces, the equilibrium equations are obtained as

$$\Big[\sum_{\ell=1}^{n} g^{(\ell)}\left(\sigma_{i'j'}^{(a)} - \tilde{\sigma}_{i'j'}^{(a)}\right)\delta\varepsilon_{i'j'}^{(a)} S_C^{*(e,\ell,r;CR)}\Big] h = \left|t_{B\hat{\imath}}^{(a)}\right| \delta\left|\underset{\sim}{\Delta}_{C\hat{\imath}}^{(a)}\right| \ell_{\hat{\imath}} ,$$

$$i,j = 1,2; \quad 1 \equiv \alpha, 2 \equiv \beta, \tag{12}$$

where $\tilde{\sigma}_{i'j'}^{(a)}$ represent average values of residual stresses which would act in the concrete between neighboring cracks if no stress transfer from the two orthogonal reinforcement bars to the surrounding concrete took place between neighboring cracks.

For one crack band only,

$$\begin{Bmatrix} \tilde{\sigma}_{1'1'}^{(a)} \\ \tilde{\sigma}_{2'2'}^{(a)} \\ \tilde{\sigma}_{1'2'}^{(a)} \end{Bmatrix} \equiv \begin{Bmatrix} \tilde{\sigma}_{\alpha'\alpha'}^{(a)} \\ \tilde{\sigma}_{\beta'\beta'}^{(a)} \\ \tilde{\sigma}_{\alpha'\beta'}^{(a)} \end{Bmatrix} = \begin{Bmatrix} 0 \\ \sigma_{\beta'\beta'}^{(a)}\left(\sigma_{\alpha'\alpha'}^{(a)} = 0\right) \\ 2\bar{G}\varepsilon_{\alpha'\beta'}^{(a)} \end{Bmatrix} \tag{13}$$

where $\bar{G}$ is taken from [10]. For two crack bands, also $\tilde{\sigma}^{(\sigma)}_{\beta'\beta'} = 0$. $S_C^{*(e,\ell,r;CR)}$ refers to integration point r.

Substitution of (10) into (1), considering (12), results in

$$\sum_{e=1}^{m}\Big[\sum_{\ell=1}^{n} g^{(\ell)}\Big(\int_{S_C^{(e,\ell;UN)}} \sigma_{l''}\,\delta\varepsilon_{i''}\,h\,dS + \int_{S_C^{(e,\ell;CR)}} \tilde{\sigma}^{(\sigma)}_{i'j'}\,\delta\varepsilon^{(\sigma)}_{i'j'}\,h\,dS\Big) + \sum_{r=1}^{r}\Big(\int_{S_{S\hat{\imath}}^{(e,r;UN)}} \sigma_{\hat{\imath}}\,\delta\varepsilon_{\hat{\imath}}\,\mu_{\hat{\imath}}\,h\,dS +$$

$$+\int_{S_{S\hat{\imath}}^{(e,r;CR)}} f_{\hat{\imath}}\,\sigma^{(\sigma)}_{\hat{\imath}}\,\delta\varepsilon^{(\sigma)}_{\hat{\imath}}\,\mu_{\hat{\imath}}\,h\,dS\Big) - \int_{V^{(e)}} \bar{\rho}g\,\delta u_g\,dV - \int_{S_p^{(e)}} \rho g\,\delta u_g\,dS\Big] - \sum_{b=1}^{a}\int_{S^{*(\ell)}} \big(\lambda_{1*}\,\delta\vartheta_{1*} + \vartheta_{1*}\,\delta\lambda_{1*}\big)\,ds^* = 0, \tag{14}$$

$$g = 1,2,3; \quad i,j = 1,2; \quad 1\equiv\alpha,\ 2\equiv\beta,\ 3\equiv\nu,$$

where

$$f_{\hat{\imath}} = 1 + \frac{|\tau^{(\sigma)}_{B\hat{\imath}}|}{\sigma^{(\sigma)}_{S\hat{\imath}}}\,\frac{\{b_{1'}\}}{\{\ell_{\hat{\imath}}\}}\,\frac{}{\phi_{\hat{\imath}}}\sum_{\ell=1}^{n} g^{(\ell)}\Big(1 + \frac{12\,\nu_{S\hat{\imath}}}{h^2}\,\nu_C^{(\ell)}\Big)\,\frac{\{b_{1'}\}}{\ell_{\hat{\imath}}^{(\ell)}} \tag{15}$$

is termed tension-stiffening factor. Upper (lower) quantities in brackets refer to parallel cracks in one (two) directions.

For the limiting case of zero steel stress at $s_{\hat{\imath}} = 0$, that is, for point B in the plot at the bottom right of Fig.3 coinciding with point A, $\sigma^{(CR)}_{S\hat{\imath}} = 2\sigma^{(\sigma)}_{S\hat{\imath}}$. Thus,

$$1 \le \frac{\sigma^{(CR)}_{S\hat{\imath}}}{\sigma_{S\hat{\imath}^{(\sigma)}}} \le 2, \tag{16}$$

resulting in the following bounds for $f_{\hat{\imath}}$ [4]:

$$1 \le f_{\hat{\imath}} \le 1 + \begin{Bmatrix} |n_{1'\hat{\imath}}| \\ 1 \end{Bmatrix}\sum_{\ell=1}^{n} g^{(\ell)}\Big(1 + \frac{12\,\nu_{S\hat{\imath}}}{h^2}\,\nu_C^{(\ell)}\Big)\,\frac{\{b_{\nu}\}}{\ell_{\hat{\imath}}^{(\ell)}}\ . \tag{17}$$

2.3. Incremental-Iterative FE Analysis

For ultimate load analysis of RC surface structures, the load must be applied incrementally. The resulting incremental internal forces are computed with the help of incremental equations of equilibrium, following from (14). In order to reduce the unbalance between external and internal forces, equilibrium iterations are performed at each load increment. Details of the incremental-iterative FE analysis are given in [4]. Details of the employed finite element may be found in [11].

3. NUMERICAL INVESTIGATION

The developed concept for consideration of tension stiffening is applied to an experimental RC panel and an experimental RC shell within the framework of ultimate load analyses.

3.1. RC Panel

The experimental panel shown in Fig.6 is considered. This panel was tested by Leonhardt and Walther [12] and analyzed by Cedolin and Dei Poli [13]. For the present analysis the panel is divided into three subregions of different material properties (subregions 1, 2, 3 in the right half of Fig.6). Material properties are listed in Table 1. The increase of the value for f_{cu} in the vicinity of the supports (subregion 3) should account for the local increase of panel strength, resulting from steel wires of 2mm diameter, helically wrapped round each pair of horizontal hooks at both ends of the main reinforcement [2]. Because of symmetry, only one half of the panel needs to be considered for the analysis. The FE model consists of 72 triangular elements. Cubic interpolation polynomials are chosen as mode shapes for the element displacement functions [11].

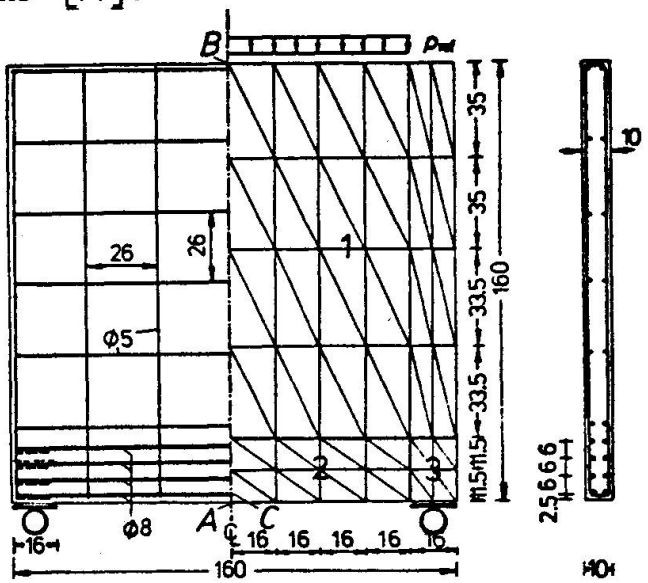

φ5(8) ≙ diameter of reinforcement steel: 5 (8) mm
dimensions of panel in cm
p_{ref} = 1.6406 kN/cm

Fig.6 Experimental RC Panel (Ref. 12) - Finite Element Model

Table 1 Material Properties for Panel

Concrete			Steel		
$E_C^{(0)}$	3200	kN/cm²	$E_S^{(0)}$	2100	kN/cm²
ν_C	0.20	—	$E_S^{(h)}$	0	kN/cm²
$f_{cu}^{(1,2)}$	-3000	N/cm²	$\phi_x^{(1)} = \phi_y$	0,5	cm
$f_{tu}^{(1,2)}$	300	N/cm²	$f_{SY}^{(I)}$	±24000	N/cm²
$f_{cu}^{(3)}$	-4000	N/cm²	$\phi_x^{(2,3)}$	0.8	cm
$f_{tu}^{(3)}$	400	N/cm²	$f_{SY}^{(II)}$	±54700	N/cm²

Arabic Superscripts Denote Subregions of Panel (See Fig.6)
Roman Superscript Indicates Steel Quality for Above Listed Bars

Fig.7 contains diagrams of the vertical displacement v at point A (see Fig.6) as a function of the load intensity factor $\chi = P/P_{ref}$, where Pref = $p$ref • 128cm = 210 kN is the resultant of $p$ref (see Fig.6). The diagram resulting from the experiment seems to indicate that the failure load is lower than the analytically obtained failure load in case of consideration of tension stiffening. In this context it should be mentioned that after initial failure at $\chi = 4.5$ in the vicinity of the left support, caused by improper consolidation of concrete, steel bandages were pressed sideways against the damaged part of the panel and the experiment was continued. At $\chi = 6.0$, failure also occurred in the vicinity of the right support, caused by fracturing of concrete [12]. Unfortunately, the continuation of the load-displacement diagram beyond initial failure is not reported in [12].

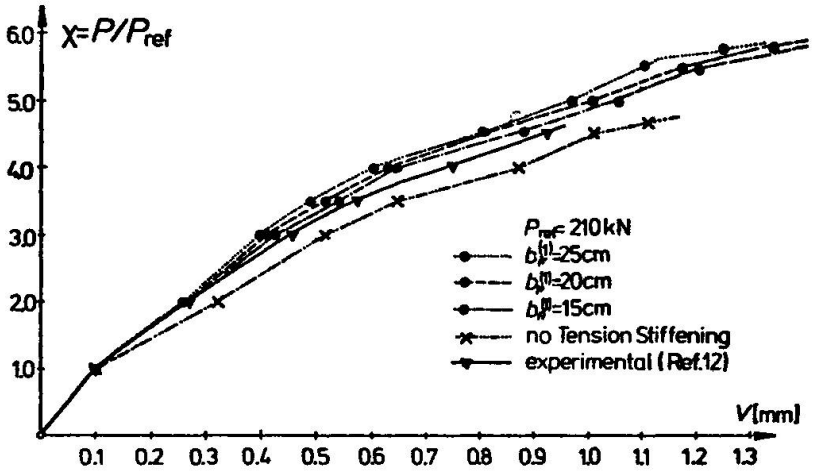

Fig.7 Vertical Displacement v of Point A versus load Intensity Factor χ

It is seen that the experimental failure load is reproduced by the analysis in case tension stiffening is considered. The load-displacement diagrams are found to be relatively insensitive to variations of the free parameter $b_f'^{(1)}$. If the tension-stiffening effect is disregarded, the failure load is underestimated by approximately 25 %.

Fig.8 shows a comparison of concrete stresses σ_{Cxx} along center line $\overline{AB}$ for three different material models at three different load intensities. The plot for $\chi = 3.0$ illustrates that, as a consequence of the tension-stiffening effect, the neutral axis experiences a shift towards the neutral axis that would be obtained in case concrete was treated in the analysis as a linear elastic, uncracked material.

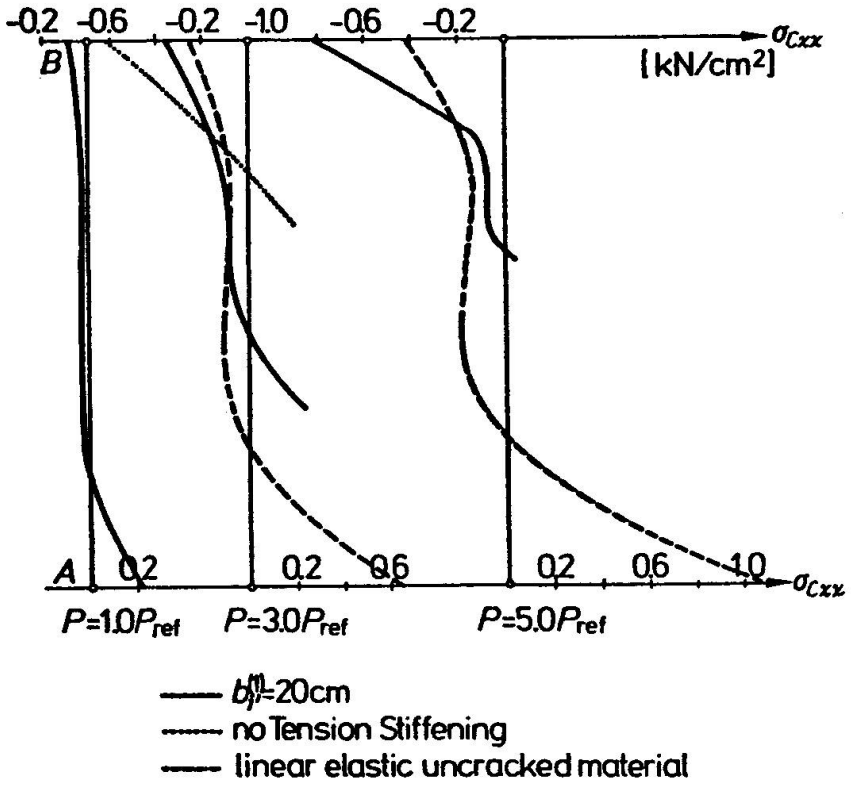

Fig.8 Comparison of Concrete Stresses σ_{Cxx} Along Center Line $\overline{AB}$ for Three Different Load Intensities

Fig.9 shows diagrams of the steel stress σ_{Sx} in the bottom main reinforcement at point C versus the load intensity factor χ . In case of consideration of the tension-stiffening effect, the results

of the writers agree well with the experimental results. This follows from consideration of average stresses in the experiment as well as in the analysis.

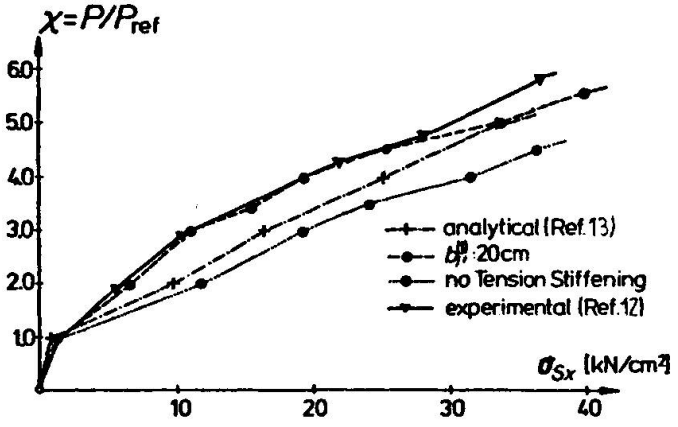

Fig.9 Stress σ_{Sx} in Main Reinforcement at Point C versus Load Intensity Factor χ

3.2. Parabolically - Cylindrical RC Shell

A 1: 8 model of a built barrel vault, tested by Hedgren [14] and analyzed by Lin [15], is re-analyzed by the writers. Because of

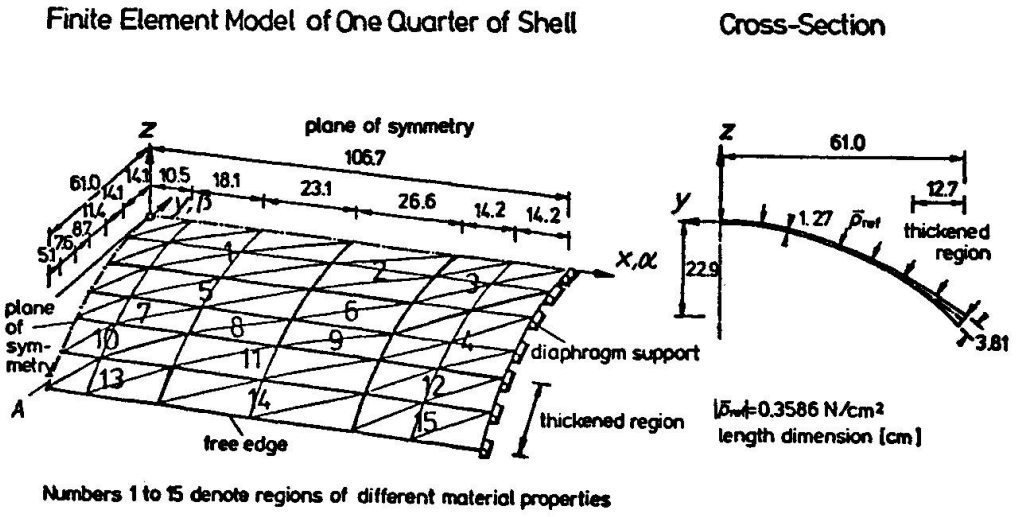

Fig.10 Experimental Parabolically - Cylindrical RC Shell (Ref.14)- Finite Element Model

symmetry, only one quarter of the shell needs to be considered for the analysis. Fig.10 shows the FE model as well as the cross section of the shell. The shell is subjected to constant hydrostatic pressure, representing a so-called "follower load".

Table 2 contains material properties. The numbers 1-15 in Fig.10 permit identification of subregions of the shell, characterized by constant material properties. Table 3 contains distances of steel layers from the middle surface of the shell, ν, referred to the thickness of the shell, h, as well as thicknesses of steel layers. For the analysis, the shell is divided into 9 concrete layers.

Table 2 Material Properties for Shell

Concrete			
$E_C^{(0)}$	2069.1		kN/cm²
ν_c	0.145		-
f_{cu}	-3027.8		N/cm²
f_{tu}	480.0		N/cm²
Steel			
Designation	Diameter [cm]	$\lvert\sigma_y\rvert$ [kN/cm²]	$\lvert\sigma_u\rvert$ [kN/cm²]
#3	0.122	25.3	36.4
#4	0.157	21.9	34.5
#9	0.343	30.7	42.0
$E_S^{(0)}$	20001.6		kN/cm²
$E_S^{(h)}$	2000.2		kN/cm²

Table 3 Steel Layers in Shell

Mat #	Bottom Longitudinal (φ=0°) ν/h	$\mu\cdot h$*	#	Bottom Circumferential (φ=90°) ν/h	$\mu\cdot h$	#	Bottom Free Edge (φ=0°) ν/h	$\mu\cdot h$	#	Middle Surface Diagonal (φ=45°) ν/h	$\mu\cdot h$	#	Top Free Edge (φ=0°) ν/h	$\mu\cdot h$	#	Top Longitudinal (φ=0°) ν/h	$\mu\cdot h$	#	Top Circumferential (φ=90°) ν/h	$\mu\cdot h$	#
1					0.014007															0.011684	
2					0.003064					-	θ	-								0.010225	
3					0.003828															0.006135	
4										0.000	0.007668	4									
5	-0.250	0.003064		-0.154	0.014007											0.140			0.250	0.005842	
6					0.003064		-	θ	-	-	θ	-	-	θ	-					0.005112	
7			3																		
8					0.007008	3				0.000	0.007668	4					0.003064	3		0.005842	4
9					0.006128															0.005112	
10										-	θ										
11	-0.312	0.006128		-0.239	0.007008					0.000	0.007668	4				0.229			0.312	0.005842	
12					0.003678						0.005112									0.006135	
13								0.058141		-	θ			0.058141							
14	-0.397	0.010225	4	-0.352	0.007008		-0.231	0.054322	9	0.000	0.007668	4	0.231	0.054322	9	0.352			0.397	0.005842	
15					0.003678			0.036215			0.005112			0.036215						0.006135	

*dimension $\mu\cdot h$ [cm]

Fig.11 shows the influence of tension stiffening on the transverse displacement w at point A (midspan of the free edge). The horizontal hatching in this figure indicates the "band width" within which the load-displacement curve obtained from the experiment is located. This band width was introduced by the writers in [4] because of the uncertainty concerning the exact location of this curve. Note that Lin [15] obtained this curve from extrapolation of Hedgren's experimental results [14]. Fig.11 illustrates that the load-displacement curve is significantly "softer" if tension stiffening is disregarded (f_t=1). In this case the failure load of the shell is underestimated.

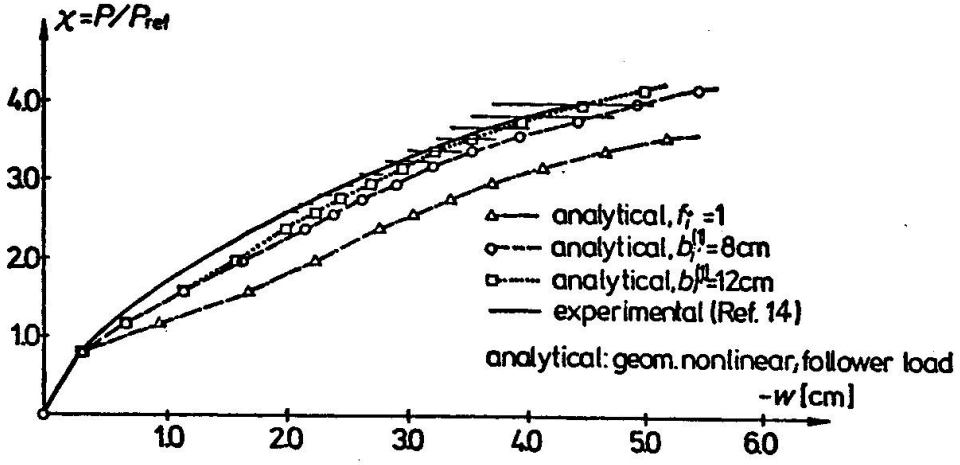

Fig.11 Transverse Displacement w at Point A versus Load Intensity Factor χ - Influence of Tension-Stiffening

Fig.12 shows the stress $\sigma_{S\alpha}$ in the bottom main reinforcement at point A as a function of the load intensity factor χ. At low load levels, the tension-stiffening effect results in a significant reduction of the steel stress.

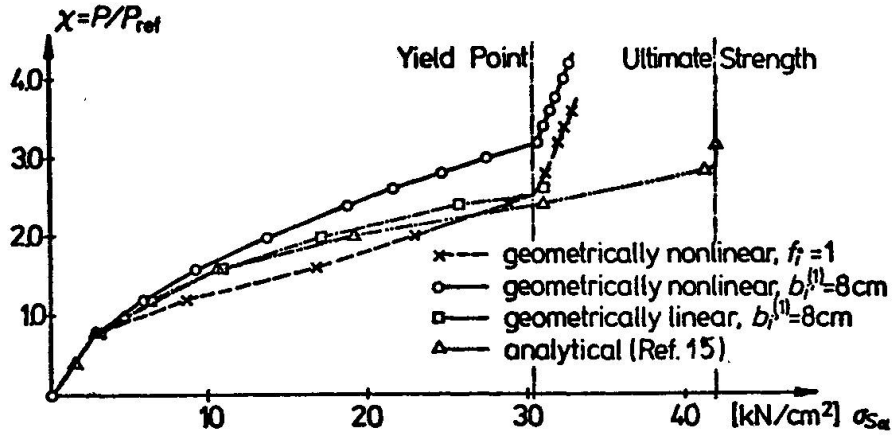

Fig.12 Stress in Bottom Main Reinforcement at Point A versus Load-Intensity Factor χ

4. CONCLUSIONS

The tension-stiffening effect is considered by means of tension-stiffening factors, representing multipliers for average values of steel stress between neighboring cracks in the equations of equilibrium. The tension-stiffening factor depends on (a) the average bond stress between neighboring cracks, (b) the angle between the normal to the crack and the intersecting reinforcement bar, (c) the degree of crack propagation through the thickness of the shell and (d) the extent of formation of secondary cracks between neighboring primary cracks. In spite of the fact that bond slip is the basis for the proposed concept, relative displacements between the reinforcement and the surrounding concrete need not be employed for the numerical analysis. Disregard of the tension-stiffening effect may result in a significant underestimation of the ultimate load. At intermediate load levels the steel stresses may be overestimated considerably. Provided a reasonable assumption is made for the initial crack spacing, results are insensitive to variation of this value.

ACKNOWLEDGEMENTS

The writers are indebted to L. Cedolin of Politecnico di Milano who devoted much of his time for introducing them to the theoretical concept and to computational details of his research on RC panels. He also made available a computer program for iterative determination of stress in the intact concrete. Many helpful discussions with W. Mudrak of Technische Universität Wien and W. Potucek of Österreichische Bundesbahn are thankfully acknowledged. Financial support of the Fonds zur Förderung der wissenschaftlichen Forschung der Republik Österreich is gratefully acknowledged.

REFERENCES

1. GILBERT, R.I.; WARNER, R.F.: Tension Stiffening in Reinforced Concrete Slabs. Proc. ASCE, J.Struct.Div. 104, 1978, 1885-1899
2. FLOEGL, H.; MANG, H.A.: Tension Stiffening Concept for RC Panels Based on Bond Slip. Manuscript Submitted for Publication in Proc. ASCE, J.Struct.Div.

3. SCANLON, A.: Time Dependent Deflections of Reinforced Concrete Slabs. Dissertation, University of Alberta, Edmonton, Canada, 1971

4. FLOEGL, H.; MANG, H.A.: On Tension Stiffening in Cracked Reinforced Concrete Slabs and Shells Considering Geometric and Physical Nonlinearity. Ing.-Arch., in print

5. KOITER, W.T.: General Equations of Elastic Stability for Thin Shells. Proc.Symp. on the Theory of Shells to Honor Lloyd Hamilton Donell, University of Houston, 1967

6. LIU, T.C.Y.; NILSON, A.H.; SLATE, F.O.: Biaxial Stress-Strain Relations for Concrete. Proc. ASCE, J.Struct.Div. 98, 1972, 1025-1034

7. KUPFER, H.: Das Verhalten des Betons unter mehrachsiger Kurzzeitbelastung unter besonderer Berücksichtigung der zweiachsigen Beanspruchung. Report, Deutscher Ausschuß für Stahlbeton, Vol. 229, Berlin, 1973

8. GRELAT, A.; POTUCEK, W.: Comportement de Panneaux en Béton précontraint soumis au Cisaillement. Report, CEBTP Paris, St. Rémy-lés-Chevr, 1978

9. FLOEGL, H.; MANG, H.: Zum Einfluß der Verschiebungsabhängigkeit ungleichförmigen hydrostatischen Drucks auf das Ausbeulen dünner Schalen allgemeiner Form. Ing.-Arch. 50, 1981, 15-30

10. CEDOLIN, L; DEI POLI,S.: Finite Element Nonlinear Plane Stress Analysis of Reinforced Concrete. Report, Costruzioni in Cemento Armato, Studi e Rendiconti, Vol. 13, Politecnico di Milano, 1976

11. MANG, H.; GALLAGHER, R.H.; CEDOLIN, L.; TORZICKY, P.: Deformation und Stabilität windbeanspruchter Kühlturmschalen. Ing.-Arch. 47, 1978, 391-410

12. LEONHARDT, F.; WALTHER, R.: Wandartige Träger. Report, Deutscher Ausschuß für Stahlbeton, Vol.178, Berlin, 1963

13. CEDOLIN,L.; DEI POLI, S.: Berechnung wandartiger Stahlbetonträger mit dem Verfahren der finiten Elemente. Beton- und Stahlbetonbau 73, 1978, 226-230

14. HEDGREN, A.W., JR.: A Numerical and Experimental Study of Translational Shell Roofs. Dissertation, Princeton University, 1965

15. LIN, C.S.: Nonlinear Analysis of RC Shells of General Form. Report, Dept. of Civ.Engng., University of California at Berkeley, 1973

16. ÅLDSTEDT, E.; BERGAN, P.G.: Nonlinear Time-Dependent Concrete-Frame Analysis. Proc. ASCE, J.Struct.Div. 104, 1978, 1077-1092

Leere Seite
Blank page
Page vide